# Analytical estimation of ATF beam halo distribution *

WANG Dou(王逗)[1] Philip Bambade[2] KaoruYokoya[3] GAO Jie(高杰)[1]

[1] Institute of High Energy Physics, Chinese Academy of Sciences, Beijing 100049, China
[2] LAL, Univ Paris-Sud, CNRS/IN2P3, Orsay, France
[3] KEK, Tsukuba, Ibaraki, Japan

**Abstract:** In order to study the backgrounds in the ATF2 beam line and the interaction point (IP), this paper has developed an analytical method to give an estimation of the ATF beam halo distribution based on K. Hirata and K. Yokoya's theory. The equilibrium particle distribution of the beam tail in the ATF damping ring is presented, with each electron affected by several stochastic processes such as beam-gas scattering, beam-gas bremsstrahlung and intra-beam scattering, in addition to the synchrotron radiation damping effects. This is a general method which can also be applied to other electron rings.

**Key words:** ATF, halo distribution, beam-gas scattering, beam-gas bremsstrahlung, intra-beam scattering

**PACS:** 29.20.db **DOI:** 10.1088/1674-1137/38/12/127003

## 1 Introduction

The distribution function of an electron bunch, transverse or longitudinal, is often assumed to be Gaussian. Actually, however, due to stochastic processes, there always exists some deviation and hence charge distributions of accelerator beams can be separated into two parts: the beam cores, which usually have Gaussian-like distributions, and the beam halos, which have much broader distributions than the beam cores. The central part affects the luminosity of colliders, circular or linear, and the brightness of synchrotron light sources,while the halos can give rise to background in collision experiment detectors and even reduce the lifetime if its distribution is too large.

At the interaction point (IP) of ATF2 (Accelerator Test Facility 2), an elaborately designed beam size monitor based on laser interferometer technology, called the Shintake monitor, is utilized to measure the sub-100 nm electron beam size [1]. The photon background in the IP section will influence the modulation of the Shintake monitor, however, and hence degrade the resolution of beam size measurements. Since beam halo scattering with the beam pipe is the main source of background, in order to study the charge distribution of the beam halo along the ATF2 beam line and develop a collimation strategy, we need to know the halo status at the entrance of ATF2 and furthermore, how it is generated in the ATF damping ring. So, in this paper, we try to make an analytical estimation of the halo distribution in ATF due to several common stochastic processes, based on the theory established by K. Hirata and K. Yokoya [2]. Typical damping ring parameters are listed in Table 1 [3].

Table 1. Typical ATF parameters.

| | |
|---|---|
| energy $E_0$/GeV | 1.28 |
| natural energy spread $\delta_0$ | $5.44\times10^{-4}$ |
| energy acceptance | 0.005 |
| average $\beta_x/\beta_y$/m | 3.9/4.5 |
| horizontal emittance/nm | 1 |
| vertical emittance/pm | 10 |
| transverse damping time/ms | 18.2/29.2 |
| longitudinal damping time/ms | 20.9 |

## 2 Beam-gas scattering

The performance of accelerators and storage rings depends on the many components of the accelerator, and one very important component is the vacuum system. Interactions between the accelerated particles and the residual gas atoms may degrade the beam quality. The lifetime may be reduced and/or the emittance may increase. The beam halo is possibly generated because the particles' distribution deviates from a Gaussian distribution.

The deflection of an electron via the Coulomb interaction is described by Rutherford scattering. We assume that this scattering is elastic and that the recoil momentum of the residual gas is negligible. The differential cross-section of the electron scattering with an atom is

Received 6 November 2013, Revised 5 May 2014
∗ Supported by National Foundation of Natural Science (11175192) and France China Particle Physics Laboratory (FCPPL)

given by [4]

$$\frac{\mathrm{d}\sigma}{\mathrm{d}\Omega}=\left(\frac{2Zr_{\mathrm{e}}}{\gamma}\right)^2\frac{1}{(\theta^2+\theta_{\mathrm{min}}^2)^2}, \tag{1}$$

where $Z$ is the atomic number, $r_{\mathrm{e}}$ is the classical electron radius, $\gamma$ is the relativistic Lorentz factor and $\theta_{\mathrm{min}}$ is determined by the uncertainty principle as

$$\theta_{\mathrm{min}}=\frac{Z^{1/3}\alpha}{\gamma}, \tag{2}$$

where $\alpha$ is the fine structure constant. If we integrate over the whole space angle $\Omega$, we obtain the total cross-section

$$\begin{aligned}\sigma_{\mathrm{tot}} &= \int_0^{2\pi}\int_{\theta_{\mathrm{min}}}^{\pi}\left(\frac{2Zr_{\mathrm{e}}}{\gamma}\right)^2\frac{1}{(\theta^2+\theta_{\mathrm{min}}^2)^2}\sin\theta\mathrm{d}\theta\mathrm{d}\varphi\\ &\approx 4\pi Z^{4/3}(192r_{\mathrm{e}})^2.\end{aligned} \tag{3}$$

We then need to get the probability density function $f(\theta)$. Assuming $\theta^2=\theta_x^2+\theta_y^2$, then integrating over one direction will give the differential cross-section for the other direction

$$\frac{\mathrm{d}\sigma}{\mathrm{d}\theta}=\frac{4\pi r_{\mathrm{e}}^2Z^2}{\gamma^2}\frac{1}{(\theta^2+\theta_{\mathrm{min}}^2)^{3/2}}. \tag{4}$$

Here and hereafter we denote

$$\theta\equiv\theta_x(\theta_y). \tag{5}$$

Thus,

$$\begin{aligned}f(\theta) &= \frac{1}{\sigma_{\mathrm{tot}}}\frac{\mathrm{d}\sigma}{\mathrm{d}\theta}=\frac{\theta_{\mathrm{min}}^2}{(\theta^2+\theta_{\mathrm{min}}^2)^{3/2}}\\ &\left(\int_0^{\infty}f(\theta)\mathrm{d}\theta=1\right).\end{aligned} \tag{6}$$

For the elastic scattering, we assume that CO gas is dominant for beam-gas scattering in ATF, so that the total scattering probability in a unit time is

$$N=Q\sigma_{\mathrm{tot}}c, \tag{7}$$

where $c$ is the speed of light and $Q$ is the number of gas molecules in a unit volume, given by

$$Q=2.65\times10^{20}nP, \tag{8}$$

where $n$ is the number of atoms in each gas molecule and $P$ is the partial pressure of the gas in pascals. Here for ATF, $Z=50^{1/2}$ and $n=2$.

The collision probability of electron and gas atoms during one damping time is

$$N_\tau=N\tau, \tag{9}$$

where $\tau$ is the transverse damping time for either the horizontal or vertical direction.

Finally, one gets the beam transverse distribution as

$$\begin{aligned}\rho(X) &= \frac{1}{\pi}\int_0^{\infty}\cos(kX)\exp\left[-\frac{k^2}{2}+\frac{2}{\pi}N_\tau\right.\\ &\left.\times\int_0^1\frac{\left(\int_0^{\infty}\cos\left(\frac{k}{\sigma_0'}x\theta\right)f(\theta)\mathrm{d}\theta\right)-1}{x}\arccos(x)\mathrm{d}x\right]\mathrm{d}k\\ &= \frac{1}{\pi}\int_0^{\infty}\cos(kX)\exp\left[-\frac{k^2}{2}+\frac{2}{\pi}N_\tau\right.\\ &\left.\times\int_0^1\frac{\Theta xkK_1(\Theta xk)-1}{x}\arccos(x)\mathrm{d}x\right]\mathrm{d}k,\end{aligned} \tag{10}$$

where $\Theta$ is the minimum scattering angle normalized by angular beam size, which is defined by

$$\frac{\theta_{\mathrm{min}}}{\sigma_0'}\left(\sigma_0'=\frac{\sigma_0}{\overline{\beta}}\right),$$

and $X$ denotes both horizontal and vertical normalized coordinate. This formula tells us that the beam distribution disturbed by the beam-gas scattering effect is decided by only two parameters, the normalized scattering frequency $N_\tau$ and the minimum normalized scattering angle $\Theta$. The transverse beam distributions according to Eq. (10) are plotted in Fig. 1 and Fig. 2.

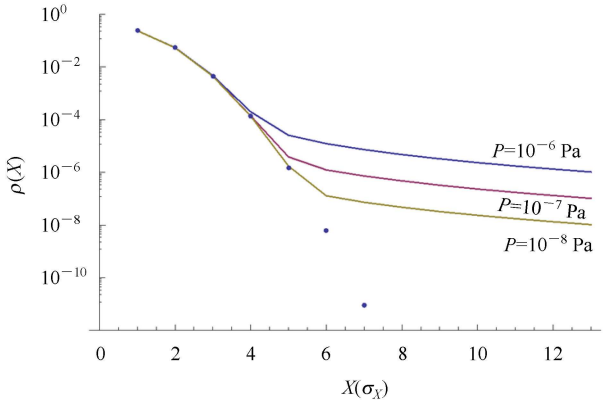


Fig. 1. Horizontal beam distribution with different vacuum pressures (horizontal coordinate $X$ is normalized by RMS beam size).

From Fig. 1 and Fig. 2, we can see that due to the beam-gas scattering effect, the beam distribution will deviate from a Gaussian distribution. A worse vacuum status will give a larger beam halo and a smaller Gaussian beam core. Also, it can be seen that the vertical distribution of a beam is affected more than the horizontal distribution by the elastic beam-gas scattering because $\sigma_{y0}'<\sigma_{x0}'$, so $\Theta_y>\Theta_x$.

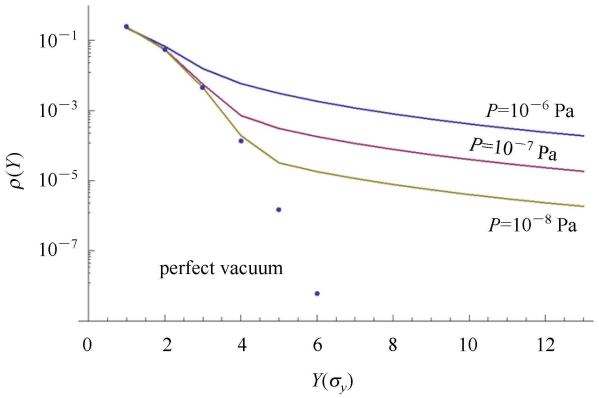


Fig. 2. Vertical beam distribution with different vacuum pressures (vertical coordinate $Y$ is normalized by RMS beam size).

## 3 Beam-gas bremsstrahlung

As is well known, when charged particles are accelerated, they emit electromagnetic radiation, i.e. photons. In accelerators, an electron with energy $E_0$, which passes a molecule of the residual gas, is deflected in the electric field of the atomic nucleus. The electron loses energy due to the radiation emitted when an electron is deflected. This bremsstrahlung will be very strong for relativistic electrons. There is a certain probability that a photon with energy $\varepsilon$ is emitted and the differential cross-section for an energy loss $\varepsilon$ due to bremsstrahlung is given by [5]

$$\frac{\mathrm{d}\sigma}{\mathrm{d}\varepsilon}=4\alpha r_{\mathrm{e}}^2 Z(Z+1)\left(\frac{4}{3}\ln\frac{183}{Z^{1/3}}+\frac{1}{9}\right)\frac{1}{\varepsilon}. \tag{11}$$

Then, one can get the total scattering frequency

$$\sigma_{\mathrm{tot}} = \int_{E_{\min}}^{E_{\max}}\frac{\mathrm{d}\sigma}{\mathrm{d}\varepsilon}\mathrm{d}\varepsilon=4\alpha r_{\mathrm{e}}^2 Z(Z+1) \times\left(\frac{4}{3}\ln\frac{183}{Z^{1/3}}+\frac{1}{9}\right)\ln\frac{E_{\max}}{E_{\min}} \tag{12}$$

and the probability density function

$$f(\varepsilon) = \frac{1}{\sigma_{\mathrm{tot}}}\frac{\mathrm{d}\sigma}{\mathrm{d}\varepsilon}=\frac{1}{\ln\dfrac{E_{\max}}{E_{\min}}}\frac{1}{\varepsilon}\left(\int_{E_{\min}}^{E_{\max}} f(\varepsilon)\mathrm{d}\varepsilon=1\right), \tag{13}$$

where $E_{\max}$ is equal to the ring energy acceptance and $E_{\min}$ is an assumed value, which will be discussed later.

Also, using the same formulae given in Eq. (7) to Eq. (9), we can calculate the total collision frequency.

Thus, the beam energy distribution due to beam-gas bremstruhlung can be expressed by

$$\rho(E) = \frac{1}{\pi}\int_0^{\infty}\cos(kE)\exp\left[-\frac{k^2}{2}+\frac{2}{\pi}N_\tau\int_0^1\frac{\left(\dfrac{\displaystyle\int_{E_{\min}}^{E_{\max}}\cos\left(\dfrac{kx}{E_0\delta_0}\varepsilon\right)\mathrm{d}\varepsilon}{\left(\ln\dfrac{E_{\max}}{E_{\min}}\right)\varepsilon}\right)-1}{x}\arccos(x)\mathrm{d}x\right]\mathrm{d}k. \tag{14}$$

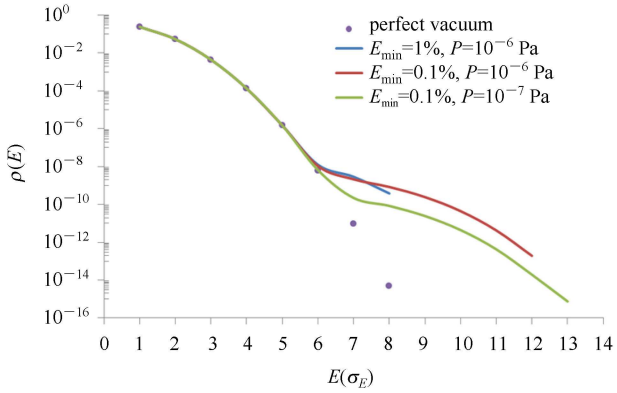


Fig. 3. Energy distribution with different vacuum pressures and different minimum energy loss (the horizontal coordinate $E$ is normalized by the naturalenergy spread).

Figure 3 shows the beam energy distribution based on Eq. (14). It can be seen that the level of the beam halo is decided by the purity of the vacuum. Lower vacuum pressure will give a smaller beam halo. Also, it shows that minimum energy loss $E_{\min}$ is an important parameter which can predict how long a tail we can get. For the ATF case, if we set a value of $E_{\min}$ larger than 1 percent of the natural beam energy spread, we will not get the distribution for the beam halo. It does not mean there are no halo particles outside 7 $\sigma_E$; it simply means the distribution function $\rho(E)$ for the energy larger than 7 $\sigma_E$ becomes negative due to the calculation algorithm. We therefore need to choose an appropriate $E_{\min}$, keeping in mind a balance of CPU computing time and halo length.

## 4 Intra-beam scattering

Intra-beam scattering (IBS) is the result of multiple small-angle Coulomb collisions between particles in the beam, which is different from the Touschek effect. The

Touschek effect describes collision processes which lead to the loss of both colliding particles. In reality, however, there are many other collisions with only small exchanges of momentum. Due to the scattering effect, beam particles can transform their transverse momenta into longitudinal momenta randomly, which leads to a continuous increase of beam dimensions and to a reduction of the beam lifetime when the particles hit the aperture. Detailed theories of intra-beam scattering have been developed in references [6–12]. However, the current theories mainly discuss the rms emittance growth and the rise time due to intra-beam scattering, which cannot give all the particle distribution information because the beam has a non-Gaussian distribution. In this paper, we will focus on the IBS induced beam distribution for the longitudinal and vertical directions.

In the center-of-mass reference frame of two scattering particles, the differential cross section of Coulomb scattering for electrons (or positrons) is given by the Möller formula [13]

$$\frac{\mathrm{d}\bar{\sigma}}{\mathrm{d}\Omega}=\frac{4r_{\mathrm{e}}^2}{(v/c)^4}\left(\frac{4}{\sin^4\theta}-\frac{3}{\sin^2\theta}\right), \tag{15}$$

where $v$ is the relative velocity in the c.m. system, which we will assume to be essentially horizontal because horizontal momentum is much larger than vertical momentum, and hence will contribute more to momentum exchange, and $\theta$ is the scattering angle. The bar denotes the center-of-mass reference frame and the differential cross section $\mathrm{d}\bar{\sigma}$ is evaluated in the center-of-mass system.

At small angles (as is common for IBS), the Möller formula for the differential cross section reduces to

$$\frac{\mathrm{d}\bar{\sigma}}{\mathrm{d}\Omega}=\frac{16r_{\mathrm{e}}^2}{(v/c)^4}\frac{1}{\sin^4\theta}. \tag{16}$$

Considering the angular change of the momentum gives a momentum component perpendicular to the horizontal axis

$$p_\perp=p_x\sin\theta, \tag{17}$$

and

$$\mathrm{d}p_\perp=p_x\cos\theta\mathrm{d}\theta\approx-p_x\mathrm{d}\theta, \tag{18}$$

with

$$p_x=\frac{m_0v}{2}, \tag{19}$$

where $m_0$ is the rest mass of the electron. Also considering

$$\mathrm{d}\Omega=2\pi\sin\theta\mathrm{d}\theta, \tag{20}$$

one can get

$$\mathrm{d}\bar{\sigma}=2\pi\frac{r_{\mathrm{e}}^2}{\bar{\beta}^2}\frac{\mathrm{d}p_\perp}{p_\perp^3}, \tag{21}$$

where $\bar{\beta}$ is the c.m. velocity of the electrons in units of $c$ $\left(\bar{\beta}=\dfrac{v}{2c}\right)$ and $p_\perp$ is the momentum exchange from the horizontal direction to the perpendicular directions in the center-of-mass frame.

Furthermore, taking account of the fact that the probability is the same for transfers occurring in the vertical and longitudinal directions, we can get the differential cross section for longitudinal momentum growth in the center-of-mass system

$$\mathrm{d}\bar{\sigma}=\pi\frac{r_{\mathrm{e}}^2}{\bar{\beta}^2}\frac{\mathrm{d}\varepsilon}{\varepsilon^3}, \tag{22}$$

where $\varepsilon$ is the longitudinal momentum change due to the IBS effect in the center-of-mass system. If we transfer the longitudinal momenta back to the laboratory system, the real longitudinal momentum growth will be $\gamma\varepsilon$.

Finally, for a single test particle, the total number of events of momentum exchange from the horizontal direction to the longitudinal direction per second and the probability density function $f(\varepsilon)$ can be written as Eq. (23) and Eq. (24).

$$\begin{aligned} N &= \frac{4\pi}{\gamma^2}\int\bar{\beta}cP(\vec{x}_1,\vec{x}_2)\int_{E_{\min}}^{\infty}\frac{\mathrm{d}\bar{\sigma}}{\mathrm{d}\varepsilon}\mathrm{d}\varepsilon\mathrm{d}\vec{x}_1\mathrm{d}\vec{x}_2 \\ &\approx \frac{cr_{\mathrm{e}}^2}{6\gamma^3}\frac{N_{\mathrm{e}}}{E_{\min}^2\sigma_x\sigma_y\sigma_z\sigma_{x'}}, \end{aligned} \tag{23}$$

$$f(\varepsilon) = \frac{1}{\bar{\sigma}_{\mathrm{tot}}}\frac{\mathrm{d}\bar{\sigma}}{\mathrm{d}\varepsilon}=\frac{2E_{\min}^2}{\varepsilon^3}. \tag{24}$$

For the integration of Eq. (23), we have used the approximate result in Ref. [10].

Thus, one gets the expression of beam energy distribution due to the IBS process as

$$\rho(E) = \frac{1}{\pi}\int_0^\infty\cos(kE)\exp\left[-\frac{k^2}{2}+\frac{2}{\pi}N_\tau\int_0^1\frac{\left(\int_{E_{\min}}^{\infty}\dfrac{2E_{\min}^2\cos\left(\dfrac{kx}{E_0\delta_0}\gamma\varepsilon\right)}{\varepsilon^3}\mathrm{d}\varepsilon\right)-1}{x}\arccos(x)\mathrm{d}x\right]\mathrm{d}k, \tag{25}$$

where $N_\tau$ is the total scattering rate normalized by the longitudinal damping rate ($N_\tau = N\tau_z$) and $E_{\min}$ is the minimum momentum increment in the longitudinal direction during the IBS process. We have explained the meaning of $E_{\min}$ and the principles for choosing its value in Section 3.

Furthermore, using the same method of beam-gas scattering, one can get the vertical distribution due to IBS as

$$\rho(Y) = \frac{1}{\pi}\int_0^\infty \cos(kY)\exp\left[-\frac{k^2}{2}+\frac{2}{\pi}N_\tau\int_0^1 \frac{\left(\int_{P_{\min}}^\infty \frac{2P_{\min}^2\cos\left(\frac{kx}{\sigma_{y'}}p_y\right)}{p_y^3}\mathrm{d}p_y\right)-1}{x}\arccos(x)\mathrm{d}x\right]\mathrm{d}k, \tag{26}$$

where $N_\tau$ is the total scattering rate normalized by the vertical damping rate ($N_\tau = N\tau_y$) and $P_{\min}$ is the minimum momentum increment in the vertical direction during the IBS process.

Figure 4 shows the beam energy distribution based on Eq. (25). Here, we choose $E_{\min}$ equal to 0.01% of natural energy spread. We can see that a larger beam density gives a larger beam halo, which will also increase the RMS beam size. Since the design bunch population is $1\times10^{10}$ for the ATF damping ring, from Fig. 4, the beam energy distribution will deviate from a Gaussian shape outside $8\sigma_E$ and the halo particles will have about $1\times10^{-16}$ of peak beam density. Compared with Fig. 3, it can be seen that in the ATF damping ring, the energy distribution of the beam halo is dominated by the beam-gas bremsstrahlung effect rather than the IBS effect.

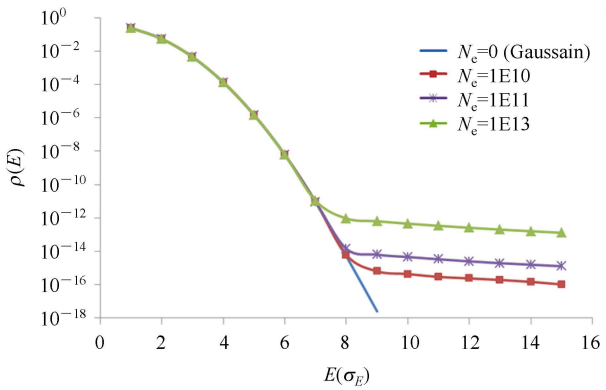


Fig. 4. Energy distribution with different bunch populations (the horizontal coordinate $E$ is normalized by the natural energy spread).

Figure 5 shows the vertical charge distribution based on Eq. (26). Here, we choose $P_{\min}$ of about 0.02% of the natural energy spread. In the ATF damping ring, the vacuum level is at the order of $10^{-7}$–$10^{-6}$ Pa. According to Fig. 2, the charge intensity of the vertical halo is about four orders of magnitude lower than at the beam center in the ATF. So it seems that in the ATF damping ring, the vertical distribution is dominated by beam-gas scattering rather than by the IBS effect.

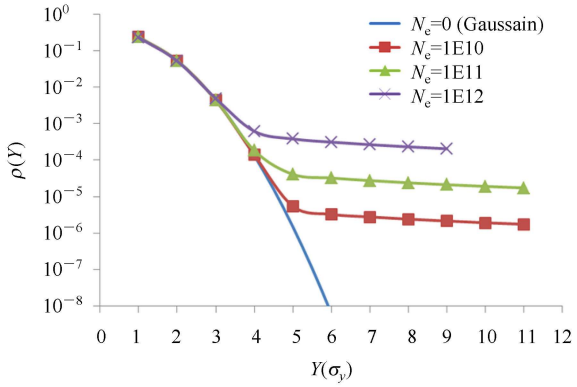


Fig. 5. Vertical distribution with different bunch populations (vertical coordinate $Y$ is normalized by RMS beam size).

## 5 Conclusions and future work

Due to various incoherent stochastic processes in the electron (positron) rings in an accelerator, the beam distribution will deviate from a Gaussian shape, generating a longer beam tail and increasing the beam dimensions. With the background issue, we have to study the halo distributions and the mechanisms by which the halo particles are produced. For the RMS emittance growth, we do have some mature theories and numerical codes to use, while for the whole beam distribution, especially for the halo part, there are few mature theories. Even using simulations, it is difficult to get the vertical RMS emittance and the halo distribution for three directions be-

cause the beam halo includes much fewer particles than the beam core. For the first time, we have analyzed the whole beam distribution of the ATF damping ring, including the halo section, looking at beam-gas scattering, beam-gas bremsstrahlung and intra-beam scattering, based on the existing theory of K. Hirata and K. Yokoya. From our study, it seems that the transverse halo in ATF is dominated by beam gas scattering while the longitudinal halo is dominated by beam gas bremsstrahlung. The analytical method developed in this paper is not specific to ATF and can be utilized on any other electron ring.

For the next step, we will study the horizontal distribution due to IBS, where a coupling effect between the longitudinal direction and the horizontal direction exists through horizontal dispersion. Also, we will study the influence of different ring emittances on the IBS process. A smaller emittance will induce a higher collision frequency but lower momentum exchange, so different emittances may give different halo shapes. In addition, we plan to develop a semi-theoretical method based on a random generator to produce the combined Gaussian core and halo distributions so that we can study the combined distribution due to different stochastic processes.

## References


1 Taikan Suehara et al. Design of a Nanometer Beam Size Monitor for ATF2. arXiv:0810.5467 [physics.ins-det]

2 Kohji Hirata, Kaoru Yokoya. Non-Gaussian Distribution of Electron Beams Due to Incoherent Stochastic Processes. Particle Accelerators, 1992, **39**: 147–158

3 Bane K L F, Hayano H, Kubo K, Naito T, Okugi T, Urakawa J. Intrabeam Scattering Analysis of Measurements at KEK's Accelerator Test Facility Damping Ring. PRSTAB, 2002, **5**: 084403

4 Heilter W. The Quantum Theory of Radiation, Oxford: Oxford University Press, 1995

5 Eun-San Kim. Estimates of the Non-Gaussian Beam-Tail Distributions and the Beam Lifetime at the Pohang Light Source. Journal of the Korean Physical Society, 2004, **44**(4): 823–829

6 Piwinski A. Intrabeam Scattering. In Proceedings of the 9th International Conference on High Energy Accelerators. Stanford, CA. 1974

7 Bjorken J, Mtingwa S. Intrabeam Scattering. Part. Accel., 1983, **13**: 115

8 Piwinski A. Intrabeam Scattering in the Presence of Linear Coupling, DESY 90-113. 1990

9 Le Duff J. Single and Multiple Touschek Effects. In Proceedings of the CERN Accelerator School: Accelerator Physics, Berlin, Germany, 14–25 Sep 1987. 114–130

10 Raubenheimer T O. The Core Emittance with Intrabeam Scattering in e+/e− Rings. SLAC-PUB-5790, Sep. 1992

11 Kubo K, Oide K. Intrabeam Scattering in Electron Storage Rings. PRSTAB, 2001, **4**: 124401

12 Kubo K, Mtingwa S K, Wolski A. Intrabeam Scattering Formulas for High Energy Beams. PRSTAB, 2005, **8**: 081001

13 Bruck H. Accelerateurs Circulaires de Particules. Presses Universitaires de France, Paris. 1966